ACTA ONCOLOGICA
2023, VOL. 62, NO. 11, 1561–1565
https://doi.org/10.1080/0284186X.2023.2266125

Taylor & Francis
Taylor & Francis Group

LETTER TO THE EDITOR

Parameters for proton minibeam radiotherapy using a clinical scanning beam system

Fardous Reaz[a,b], Mateusz Krzysztof Sitarz[b], Erik Traneus[c] and Niels Bassler[a,b]

[a]Department of Clinical Medicine, Aarhus University, Aarhus, Denmark; [b]Danish Centre for Particle Therapy, Aarhus University Hospital, Aarhus, Denmark; [c]RaySearch Laboratories AB, Stockholm, Sweden

ARTICLE HISTORY Received 26 May 2023; Accepted 28 September 2023

Introduction

Spatially fractionated radiotherapy (SFRT) has emerged as a promising strategy for enhancing the effectiveness of external beam radiotherapy. By application of heterogeneous dose distributions within the irradiated volume, SFRT aims to mitigate severe post-radiation effects, minimise tumor regression, and improve local control [1–5]. Among the different forms of SFRT, proton minibeam radiotherapy (pMBRT) with (sub-)millimeter beam size has been proposed as a means to further optimise proton therapy by reducing toxicity and expanding the therapeutic window [6]. The advantages of pMBRT to supplement conventional proton therapy have been highlighted in several previous studies [6–11]. However, before considering pMBRT for routine clinical application, it is crucial to establish its clinical efficacy through pre-clinical studies and to define a set of reference parameters that can effectively characterise and quantify its efficacy. We are in the process of gathering new data on the biological effectiveness of pMBRT, where we intend to use the *in vivo* setup recently described [12].

Among various techniques, a metal collimator with a series of apertures is commonly used to achieve the desired irradiation profile for pMBRT [13,14]. Additionally, scanning dynamic collimators [15] and magnetically shaped beams are also proposed [16]. However, considering the limitations and the technological complexity, a static mechanical collimator represents a simpler and possibly more feasible solution. The work presented here, is in the context of a multi-slit collimator (MSC), which is optimised for the aforementioned *in vivo* setup [12].

In this study, we refine an existing parameter of pMBRT, the center-to-center (CTC) distance, and define 'throughput' for collimated pMBRT irradiation. We explored the effects of these parameters by modeling several versions of our slit-collimator at the DCPT Varian ProBeam pencil beam scanning system (PBS). Furthermore, we introduce a new parameter, called the 'Grid Factor' (GF), to be able to quantify the biological efficacy of pMBRT with a uniform target dose. It must be stressed that in spite of the promising results for achieving tumor control with heterogeneous dose distributions in the planning target volume (PTV), we here work with homogenous tumor dose only, since we think this will simplify the biological characterisation and lead to quicker clinical adaptation.

Through a systematic investigation of the pertinent parameters of pMBRT, we can improve the reporting format and contribute to the standardisation of pMBRT/SFRT parameters. This comprehensive approach will possibly expedite pre-clinical studies.

Eventually, reducing the toxicity in the entrance region is useful for side effect reduction, or enabling dose-escalation to tumors. We foresee that pMBRT with homogenous PTV could thus be relevant for treating targets near organs at risk, or also recurrent cancers where normal tissues should be spared as much as possible.

Characterising pMBRT profiles

Valley-to-peak dose ratio (VPDR)

The Valley-to-Peak Dose Ratio (VPDR) is a dosimetric parameter expressing spatial dose homogeneity. It is defined as the ratio between the dose at the valley region (D_{valley}), and the dose at the peak region (D_{peak}), as expressed by Equation (1). The VPDR ranges between 0 and 1, with a lower value indicating a more pronounced dose contrast between the peaks and valleys.

$$\mathrm{VPDR} = \frac{D_{valley}}{D_{peak}} \tag{1}$$

The main objective of SFRT is to achieve a low VPDR (close to zero) within the normal tissue, indicating a significant dose contrast between the peaks and valleys. Simultaneously, a VPDR value of 1 is required within the PTV to ensure a uniform target dose in accordance with traditional radiotherapy practices.

In most publications, the reciprocal of VPDR, known as Peak-to-Valley Dose Ratio (PVDR), is used. However, PVDR becomes numerically unstable as the valley dose approaches zero, eventually tending towards infinity. This instability often leads to large numerical fluctuations that do not

CONTACT Fardous Reaz fardous@clin.au.dk Department of Clinical Medicine, Aarhus University, Aarhus, Denmark

meaningfully correspond to any observed effect. VPDR can serve as a more reliable and robust dosimetric parameter.

Center-to-center distance (CTC)

The CTC in SFRT refers to the distance between two consecutive peaks or valleys. Generally, the CTC is a 3D metric that depends on the depth and lateral position, particularly for non-parallel beams [14,17,18].

Two distinct types of CTC can be identified. The first, termed as the *geometrical CTC*, corresponds to the period of the collimator. For non-parallel beams, however, the geometrical CTC will not necessarily coincide with the actual CTC since the lateral distance between the dose peaks (or valleys) varies as a function of beam depth. Therefore, a clarification is needed, thus we add the second type as *actual CTC* (or *in situ CTC)*, so one clearly can distinguish between these two.

Throughput

'Throughput' may conveniently describe the fraction of primary protons that successfully pass through a collimator. In addition to the collimator's geometrical properties, the throughput is influenced by various beam parameters, such as spot emittance and beam deflection caused by the scanning system.

The geometrical throughput (GT) can be defined as the ratio of the aperture area ($A_{aperture}$), which represents the area unobstructed by the collimator material, to the total area encompassing the septa (A_{septa}) and aperture at the exit side of the collimator. Mathematically, it can be expressed as:

$$GT = \frac{A_{aperture}}{A_{aperture} + A_{septa}} \tag{2}$$

GT alone cannot fully quantify the actual fraction of the primary proton fluence passing through the collimator, particularly for realistic non-parallel beams. To address this limitation, we introduce the concept of 'Actual Throughput' (AT). This metric signifies the fraction of primary protons that effectively navigate through the collimator. AT can be calculated using Monte Carlo (MC) methods and can vary laterally for non-parallel beams delivered by a PBS. Experimentally, AT can be determined by measuring the beam current ratio both immediately before and immediately after its passage through the collimator. Another approach is to compare the beam current at a specific point with and without the collimator in place. Thus, AT is a 2D metric that varies laterally and is influenced by the proton energy, making it specific to each treatment plan and describes the loss of the beam in the collimator.

Quantifying pMBRT biological effects

For pMBRT there is a need for quantifying biological effects in meaningful and robust ways. While the clinical potential of a heterogeneous tumor dose is often suggested, this new approach still faces substantial biological characterisation work. Therefore, we here pursue a uniform target dose that can facilitate the seamless translation of pMBRT into clinics. We are not presenting biological results in this study, but to do this in the future, we introduce the GF, which can characterise the biological effectiveness of pMBRT when PTV dose coverage is homogenous. GF is here defined as the ratio of a reference homogeneous PTV dose without any collimator to the homogenous PTV dose with a collimator present, but what will give the same biological effect *at a given point of interest* along the beam:

$$GF = \left.\frac{D_{ref-ptv}}{D_{grid-ptv}}\right|_{iso-response} \tag{3}$$

One key advantage of GF is that it eliminates the reliance on ambiguous dose definitions within the heterogeneous dose region, providing a more robust and reliable evaluation. Additionally, being a ratio of doses, GF allows for direct multiplication with the planned target volume (PTV) dose, enabling an accurate assessment of dose escalation possibilities that can be achieved by implementing a pMBRT dose distribution.

Another aspect is the anticipated scaling behavior of GF in relation to the VPDR. Specifically, when VPDR is unity, GF is also unity. This congruence provides a valuable reference point for the biological effectiveness of pMBRT. In cases where pMBRT exhibits enhanced biological efficacy, GF is hypothesised to decrease well below 1 when VPDR approaches zero, establishing a clear and intuitive correlation between the physical properties of a collimator and its corresponding biological outcomes.

The definition of GF bears striking similarities to the concept of relative biological effect (RBE), further reinforcing its relevance and applicability in radiation therapy research and clinical practice. By leveraging GF, researchers, and practitioners can gain insights into the intricate relationship between dose distribution and the resulting biological effects, thereby advancing the optimisation and effectiveness of pMBRT.

Method

We conducted MC simulations using the Geant4 version 11.3 [19] tool to model the beam delivery mode of the Varian ProBeam PBS system installed at the Danish Center for Particle Therapy (DCPT), Aarhus, Denmark. The beam model [20] underwent validation against experimental data obtained from DCPT treatment rooms [21].

We simulate the mice irradiation setup used at DCPT [12,22,23] and adopted the 'QGSP_BIC_HP_EMY' physics list, which has been recommended in previous studies [24–26]. A treatment plan prepared with the Eclipse treatment planning system was simulated. The plan encompassed eight energy layers spanning from 84.7 MeV to 107.6 MeV, ensuring longitudinal uniformity with a Gaussian energy spread of 1.09% to 1.21%. The PTV represented the target volume for non-collimated irradiation and possessed dimensions of 100 mm $\times$ 25 mm $\times$ 30 mm.

The initial treatment plan was designed to provide a uniform PTV dose using a non-collimated setup, as the TPS

cannot optimise a plan with a collimator in place. However, the introduction of a collimator can compromise dose homogeneity, particularly by increasing the relative weight of lower energy layers. The plan was modified manually to deliver longitudinally uniform PTV upon insertion of the collimator using the AT of each energy layer.

We utilised the treatment plan's specifications along with the DCPT's MC beam model [20] to generate the phase-space for primary particles, also incorporating the beam deflection produced by the beam scanning magnets. The beam model included energy-dependent parameters, spot size, divergence, and covariance, which establishes the correlation between the spatial and angular distribution of phase-space. The MSC cuts out a small segment of the beam emittance, which emphasises the need for realistic modelling of the initial beam.

To evaluate SFRT parameters, the MSC was introduced 30 mm upstream from the iso-center plane in simulations, with the entrance surface of the phantom placed at the iso-center plane. Dose from all particles, fluence of all protons (primary and secondary), and neutron fluence were scored.

Results

The impact of collimator thickness, GT, and geometrical CTC on the AT is illustrated in Figure 1. Varying the collimator thickness significantly affects the number of outgoing protons, even when maintaining a consistent GT. The AT demonstrates a sharp decline up to a thickness of 20 mm, followed by a gradual decrease that is linearly proportional to the thickness. While the influence of GT on AT is less pronounced, it still exerts a noticeable effect. At approximately 45% GT, two throughput values coincide, with AT slightly higher for lower GT values and vice versa. Additionally, the geometrical CTC influences the AT. Initially, there's a sharp increase in AT from ∼35% to ∼48% as the geometrical CTC varies from 0.4 to 1.2, followed by a more gradual ascent.

The energy-dependent AT of each energy layer is a useful parameter for plan optimisation to ensure uniform PTV dose in the presence of an MSC. In Figure 2, we have shown the plan optimisation principle. The energy-dependent AT is calculated from the relative number of protons obtained before and after the collimator. The weight of each energy layer of the original plan was multiplied by a factor derived from AT to deliver a uniform PTV dose using collimated beams.

The simulated results in Table 1 offer insights into neutron yield, throughput, and VPDR, considering their dependency on pMBRT parameters obtained for MSCs. The neutron yield exhibits variations that are influenced by several factors, including thickness, geometrical CTC, throughput, and material of collimators. Specifically, as the GT increases, it correspondingly raises AT, resulting in a decrease in the neutron yield, suggesting a lower fractional absorption of primary protons in an MSC. The neutron yield levels are influenced by variations in geometrical CTC values. With a given GT of 50%, as CTC increases from 1.2 mm to 2.8 mm, a small increment in neutron yield is observed. Additionally, the attenuation of proton beams increases with the collimator's length, thereby reducing AT, even though the GT remains constant. The VPDR at 0 mm exhibits a decreasing trend with increasing collimator thickness, indicating a superior dose contrast at the surface of the phantom. However, the VPDR at 70 mm is ∼1 and remains relatively constant for different thicknesses, indicating a laterally homogeneous PTV dose.

Discussion

Achieving a uniform dose distribution at the PTV provides a straightforward method to assess the potential biological advantages of pMBRT compared to conventional proton radiotherapy. This assessment can be facilitated by using the GF derived from the physical (and homogenous) dose in the PTV. Utilising the GF can offer an advantage over quantifying heterogeneous dose distributions, which can be challenging and potentially ambiguous to define accurately. Similar to RBE, GF is anticipated to depend on tissue type and endpoint, which calls for extensive biological assessments in the future.

By incorporating a realistic beam model, it is possible to examine the influence of collimators on the spatial distribution of the dose and other subsequent effects. In pMBRT, the throughputs (GT and AT) demonstrate a strong correlation with neutron yield (see Table 1), serving as a direct indicator of the irradiated material within the collimator, also

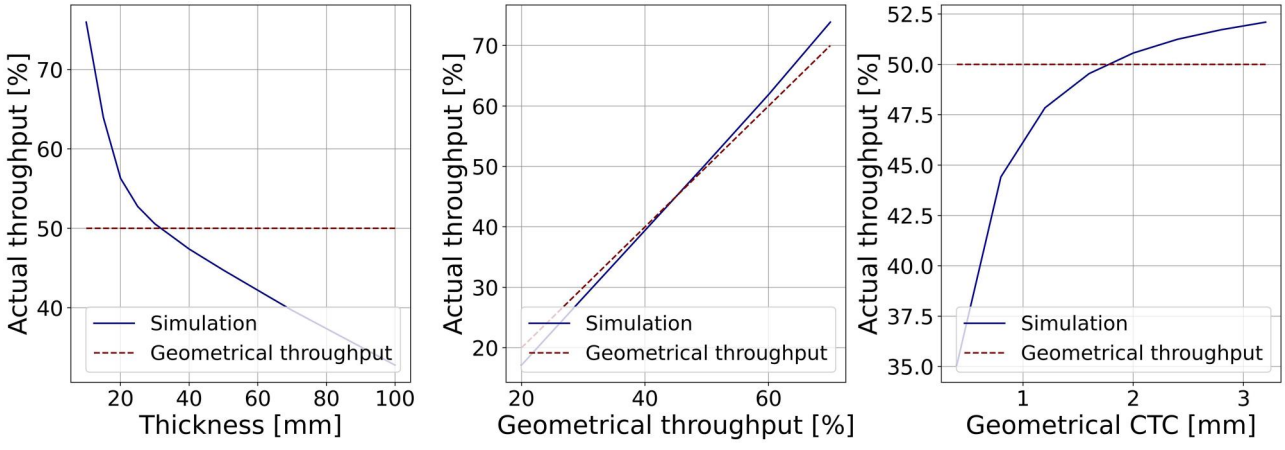

Figure 1. Impact of the thickness (left), GT (Middle), and geometrical CTC (right) on the actual throughput generated by tungsten MSC of 30 mm thickness.

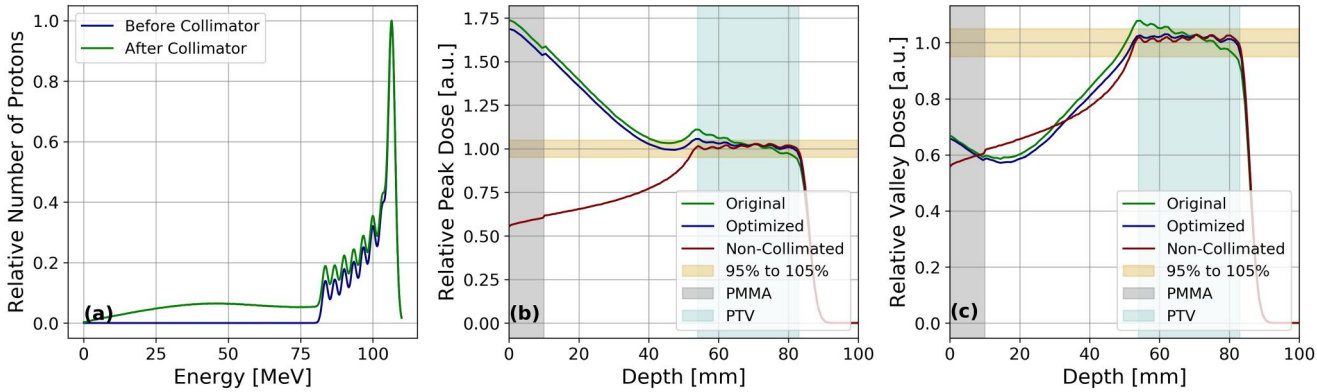

Figure 2. (a) Energy spectra of proton beam before and after a collimator. The number of protons is normalised to the peak value of the maximum energy layer. Panel (b) and (c) show depth-dose curves (at peak and valley) with and without collimator, non-optimised, and optimised for homogenous dose in the PTV for the *in vivo* setup described in Overgaard et al. [12].

Table 1. Simulated data for a water phantom starting at the iso-center plane ($z = 0$), and the edge of the MSC facing the iso center positioned at $z = -30$ mm.

Thickness (mm)	Material	CTC [mm]	GT [%]	VPDR (at 0 mm)	VPDR (at 70 mm)	AT [%]	Neutron Yield [%]
15	Tungsten	2.0	50	0.275	0.998	63.948	25.960
20	Tungsten	2.0	50	0.178	0.999	56.303	28.084
25	Tungsten	2.0	50	0.148	1.001	52.756	28.498
30	Tungsten	2.0	50	0.145	1.004	50.566	28.576
40	Tungsten	2.0	50	0.148	0.998	47.394	29.080
50	Tungsten	2.0	50	0.160	1.007	44.735	30.195
30	Tungsten	2.0	20	0.134	0.998	17.130	67.852
30	Tungsten	2.0	30	0.149	1.001	28.309	52.011
30	Tungsten	2.0	40	0.144	1.005	39.422	39.033
30	Tungsten	2.0	50	0.145	1.005	50.561	28.596
30	Tungsten	2.0	60	0.167	1.003	61.878	20.151
30	Tungsten	2.0	70	0.243	1.000	73.865	13.304
30	Tungsten	1.2	50	0.340	1.000	47.844	30.879
30	Tungsten	1.6	50	0.201	0.999	49.539	29.450
30	Tungsten	2.0	50	0.146	1.007	50.559	28.595
30	Tungsten	2.4	50	0.121	0.995	51.241	28.043
30	Tungsten	2.8	50	0.110	0.972	51.719	27.684
20	Nickel	2.0	50	0.328	0.990	68.667	7.761
20	Lead	2.0	50	0.433	1.001	80.373	18.227
20	Brass	2.0	50	0.383	0.997	74.697	10.612
20	Tungsten	2.0	50	0.173	1.002	56.296	28.075
20	Gold	2.0	50	0.183	1.000	56.660	27.499

VPDR is shown for two depths. Relative neutron yield is calculated as the ratio between the number of secondary neutrons over the total number of particles in a collimated beam and is correlated with both GT/at and the choice of material.

suggesting its potential scaling with nuclear activation of the collimator. Therefore, we think introducing these quantities is meaningful. A method to reduce slit-collimator-generated neutron dose was discussed and was also subject to optimisations to reduce the risk of secondary cancers in patients [27]. Consideration of the total particle fluence ratio between collimated and non-collimated configurations becomes crucial for achieving an equivalent prescription dose to the target volume (PTV). Moreover, energy-dependent AT is useful to reoptimise treatment plans to deliver longitudinally uniform PTV dose. Lower GT values result in reduced exposure of normal tissue volume and increased lateral dose contrast, but come at the expense of a gradual rise in secondary neutron fluence, collimator activation, and treatment delivery time, necessitating careful management. Striking a balance between achieving optimal dose distribution to the PTV, minimising collateral effects on normal tissue, and maximising beam delivery efficiency is desirable.

Our study is specific to the Varian ProBeam PBS, due to the application of the DCPT beam model. The methodology and definitions, however, can be implemented for other systems.

Conclusion

The potential advantages of pMBRT in achieving improved tumor control and reduced normal tissue toxicity have attracted significant attention within the research community. However, despite its promising prospects, there is a notable absence of standardised reporting and quantification methods for evaluating its effectiveness. To address this gap, we have examined several key parameters to further standardised reporting format for pMBRT. Notably, we introduce the concept of the 'grid factor,' which can provide an explicit measure to assess the efficacy of pMBRT with homogenous target dose.

Furthermore, we have proposed the inclusion of precise definitions for throughput and CTC as standardised field parameters. We hope to facilitate more robust evaluations of

pMBRT efficacy and improve the reliability and reproducibility of research findings.

Acknowledgements

We acknowledge support from the NovoNordisk Foundation (grant number NNF195A0059372), DCCC Radiotherapy – The Danish National Research Center for Radiotherapy WP10, and the Danish Cancer Society (Grant no. R191-A11526). We would like to thank Yolanda Prezado for her invaluable feedback during the preparation of this manuscript.

Disclosure statement

The authors declare no competing interests.

Funding

This work was supported by NovoNordisk Foundation (grant number NNF195A0059372), DCCC Radiotherapy – The Danish National Research Center for Radiotherapy WP10, and the Danish Cancer Society (Grant no. R191-A11526).

ORCID

Fardous Reaz http://orcid.org/0009-0002-8332-9655
Mateusz Krzysztof Sitarz http://orcid.org/0009-0005-6454-5354
Erik Traneus http://orcid.org/0000-0002-1850-7382
Niels Bassler http://orcid.org/0000-0002-4160-1078

Data availability statement

The datasets used and/or analysed during this study are available from the corresponding author upon reasonable request.

References

[1] Amendola B, Perez NC, Mayr N, et al. Spatially fractionated radiation therapy with lattice radiation in far-advanced bulky cervical cancer: a clinical and molecular imaging outcome study. Radiat Res. 2020;194:724–736.

[2] Choi JI, Daniels J, Cohen D, et al. Clinical outcomes of spatially fractionated GRID radiotherapy in the treatment of bulky tumors of the head and neck. Cureus. 2019;11(5):e4637. doi: 10.7759/cureus.4637.

[3] Martí Nez-Rovira I, Fois G, Prezado Y. Dosimetric evaluation of new approaches in GRID therapy using nonconventional radiation sources: dosimetric evaluation of new approaches in GRID therapy. Med Phys. 2015;42(2):685–693. doi: 10.1118/1.4905042.

[4] Snider J, Molitoris J, Shyu S, et al. Spatially fractionated radiotherapy (GRID) prior to standard neoadjuvant conventionally fractionated radiotherapy for bulky, High-Risk soft tissue and osteosarcomas: feasibility, safety, and promising pathologic response rates. Radiat Res. 2020;194:707–714.

[5] Yan W, Khan MK, Wu X, et al. Spatially fractionated radiation therapy: history, present and the future. Clin Transl Radiat Oncol. 2020;20:30–38. doi: 10.1016/j.ctro.2019.10.004.

[6] Prezado Y, Jouvion G, Patriarca A, et al. Proton minibeam radiation therapy widens the therapeutic index for high-grade gliomas. Sci Rep. 2018;8(1):16479–16410. doi: 10.1038/s41598-018-34796-8.

[7] Prezado Y, Jouvion G, Guardiola C, et al. Tumor control in RG2 Glioma-Bearing rats: a comparison between proton minibeam therapy and standard proton therapy. Int J Radiat Oncol Biol Phys. 2019;104(2):266–271. doi: 10.1016/j.ijrobp.2019.01.080.

[8] Mohiuddin M, Lynch C, Gao M, et al. Early clinical results of proton spatially fractionated GRID radiation therapy (SFGRT). Br J Radiol. 2020;93(1107):20190572. doi: 10.1259/bjr.20190572.

[9] Girst S, Greubel C, Reindl J, et al. Proton minibeam radiation therapy reduces side effects in an in vivo mouse ear model. Int J Radiat Oncol Biol Phys. 2016;95(1):234–241. doi: 10.1016/j.ijrobp.2015.10.020.

[10] Prezado Y. Proton minibeam radiation therapy: a promising therapeutic approach for radioresistant tumors. C R Biol. 2021;344(4):409–420. doi: 10.5802/crbiol.71.

[11] Lamirault C, Doyère V, Juchaux M, et al. Short and long-term evaluation of the impact of proton minibeam radiation therapy on motor, emotional and cognitive functions. Sci Rep. 2020;10(1):13511. doi: 10.1038/s41598-020-70371-w.

[12] Overgaard CB, Reaz F, Sitarz M, et al. An experimental setup for proton irradiation of a murine leg model for radiobiological studies. Acta Oncol. 2023;0:1–8. doi: 10.1080/0284186X.2023.2246641.

[13] De Marzi L, Patriarca A, Nauraye C, et al. Implementation of planar proton minibeam radiation therapy using a pencil beam scanning system: a proof of concept study. Med Phys. 2018;45(11):5305–5316. doi: 10.1002/mp.13209.

[14] Guardiola C, Peucelle C, Prezado Y. Optimization of the mechanical collimation for minibeam generation in proton minibeam radiation therapy. Med Phys. 2017;44(4):1470–1478. doi: 10.1002/mp.12131.

[15] Sotiropoulos M, Prezado Y. A scanning dynamic collimator for spot-scanning proton minibeam production. Sci Rep. 2021;11(1):18321. doi: 10.1038/s41598-021-97941-w.

[16] Schneider T, De Marzi L, Patriarca A, et al. Advancing proton minibeam radiation therapy: magnetically focussed proton minibeams at a clinical Centre. Sci Rep. 2020;10(1):1384. doi: 10.1038/s41598-020-58052-0.

[17] Ortiz R, De Marzi L, Prezado Y. Preclinical dosimetry in proton minibeam radiation therapy: robustness analysis and guidelines. Med Phys. 2022;49(8):5551–5561. doi: 10.1002/mp.15780.

[18] Kim M, Hwang UJ, Park K, et al. Dose profile modulation of proton minibeam for clinical application. Cancers (Basel). 2022;14(12):2888. doi: 10.3390/cancers14122888.

[19] Allison J, Amako K, Apostolakis J, et al. Geant4 developments and applications. IEEE Trans Nucl Sci. 2006;53(1):270–278. doi: 10.1109/TNS.2006.869826.

[20] DCPT beam model. GitHub. Available from: https://github.com/APTG/2022_DCPT_LET/tree/main/data/resources/dcpt_beam_model

[21] Lægdsmand PMT. Monte Carlo model for scanning proton beam at the Danish Center for Proton Therapy [Master thesis]. Denmark: Aarhus University; 2020.

[22] Sørensen BS, Bassler N, Nielsen S, et al. Relative biological effectiveness (RBE) and distal edge effects of proton radiation on early damage in vivo. Acta Oncol. 2017;56(11):1387–1391. doi: 10.1080/0284186X.2017.1351621.

[23] Sørensen BS, Horsman MR, Alsner J, et al. Relative biological effectiveness of carbon ions for tumor control, acute skin damage and late radiation-induced fibrosis in a mouse model. Acta Oncol. 2015;54(9):1623–1630. doi: 10.3109/0284186X.2015.1069890.

[24] Grevillot L, Frisson T, Zahra N, et al. Optimization of GEANT4 settings for proton pencil beam scanning simulations using GATE. Nucl Instrum Methods Phys Res Sect B Beam Interact Mater At. 2010;268(20):3295–3305. doi: 10.1016/j.nimb.2010.07.011.

[25] Cirrone P, Cuttone G, Mazzaglia S, et al. Hadrontherapy: a geant4-based tool for proton/ion-therapy studies. Prog Nucl Sci Technol. 2011;2:207–212.

[26] Winterhalter C, Taylor M, Boersma D, et al. Evaluation of GATE-RTion (GATE/Geant4) monte Carlo simulation settings for proton pencil beam scanning quality assurance. Med Phys. 2020;47(11):5817–5828. doi: 10.1002/mp.14481.

[27] Volz L, Reidel CA, Durante M, et al. Investigating slit-collimator-produced carbon ion minibeams with high-resolution CMOS sensors. Instruments. 2023;7(2):18. doi: 10.3390/instruments7020018.